Wake-Induced Aerodynamics on a Trailing Aircraft

Michael R. Mendenhall (AMA/NEAR)
Daniel J. Lesieutre (AMA/NEAR)
Michael J. Kelly (NASA/NESC)

ABSTRACT

NASA conducted flight tests to measure the exhaust products from alternative fuels using a DC-8 transport aircraft and a Falcon business jet. An independent analysis of the maximum vortex-induced loads on the Falcon in the DC-8 wake was conducted for pre-flight safety analysis and to define safe trail distances for the flight tests. Static and dynamic vortex-induced aerodynamic loads on the Falcon were predicted at a matrix of locations aft of the DC-8 under flight-test conditions, and the maximum loads were compared with design limit loads to assess aircraft safety. Trajectory simulations for the Falcon during close encounters with the DC-8 wake were made to study the vortex-induced loads during traverses of the DC-8 primary trailing vortex. A parametric study of flight traverses through the trailing vortex was conducted to assess Falcon flight behavior and motion characteristics.

1.0 INTRODUCTION AND BACKGROUND

NASA conducted two series of flight tests in 2013 and 2014 by the Alternative Fuel Effects on Contrails & Cruise Emissions (ACCESS) project using a NASA DC-8-72 transport jet aircraft modified to burn alternative fuel and a NASA Falcon HU-25 business jet that was specially instrumented to collect engine exhaust emission data.[(1)] The flight test is shown in Figure 1.

Figure 1. Flight Test Photograph.

Prior to the flight tests, an independent analysis of the maximum vortex-induced loads on the Falcon was conducted for pre-flight safety analysis and to define safe trail distances for the flight tests. Since there were planned excursions through the DC-8 trailing vortices by the Falcon, optimum traverse procedures were investigated to quantify the static and dynamic structural loads on the Falcon and to provide the pilots with advance information on the handling of the aircraft during these close encounters. In the initial flight tests in 2013, the Falcon pilot avoided direct contact with the DC-8 wake vortices, but in 2014 the Falcon pilot deliberately traversed the wake vortices.

One safety hazard identified with flying in close proximity to the DC-8 trailing wake vortices was structural failure of components of the airframe. This paper will describe an independent assessment of the safe trail distance of the Falcon aircraft in the wake of the DC-8 and in close proximity to the trailing vortices. The safe trail distance is that for which the Falcon component loads do not exceed 70% of the design limit loads.

2.0 TECHNICAL APPROACH

The technical approach for this independent assessment required the following tasks:

- Develop aerodynamic models for both the Falcon and DC-8 aircraft.
- Determine the DC-8 wake-induced flow field in the vicinity of the Falcon for the flight conditions.
- Predict Falcon aerodynamic characteristics and component loads under the influence of the wake.
- Compare certification loads for the Falcon to the predicted maximum induced loading from the DC-8 trailing vortices and determine a safe operating envelope.
- Evaluate Falcon flight behavior during wake vortex traverses.

The independent assessment was to be completed on an aggressive schedule prior to the flight tests. Brief descriptions of the models and prediction methods are described in this paper, but additional details are available in Refs. 2 and 3.

2.1 Aircraft Models

Aerodynamic analysis models for both the DC-8 and Falcon aircraft were created with panels, there was not the time or resources for a CFD analysis. Both aircraft were modeled in cruise and both were trimmed under free-stream flight conditions. Thrust was presumed to be equal to drag under trimmed conditions, and the center-of-gravity location was assumed to be at the quarter-chord of the mean aerodynamic chord. The nominal trim angle of attack of the DC-8 was approximately 1.35°, and the trim angle of attack of the Falcon was approximately 1.0° based on these assumptions. When the Falcon needed to be trimmed in roll under the influence of the DC-8 wake, a constant roll moment was added to the wings to counter the wake-induced rolling moment. Note that the trim conditions changed for each weight, speed, and altitude considered for the flight tests.

2.2 Trailing Vortex Models

The trailing vortex wake associated with the DC-8 must be modeled such that a realistic induced velocity field can be produced to interact with the Falcon at various locations aft of the DC-8. Traditional and proven vortex modeling techniques were selected to predict the vortex-induced velocities acting on the Falcon.[4-6]

The wake aft of the DC-8 can be represented as a distribution of discrete vortices originating along the span of the wing and horizontal tail. The DC-8 wake model used for the interference calculations in this study is a simplified model made up of a wing primary trailing vortex, several other vortices originating from the inner wing segment, and the vortex from the horizontal tail. Note that the trailing vortices are not allowed to move relative to the DC-8, and the Falcon is located relative to these fixed vortex locations. In the current model, the Falcon does not influence the position of the DC-8 vortices.

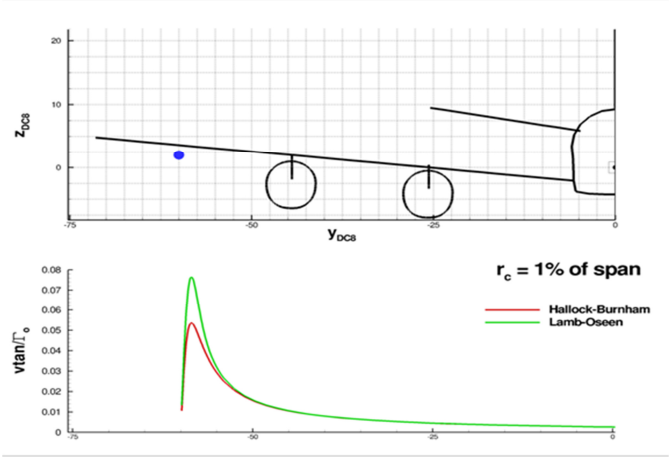

Figure 2. Velocity Profiles Through a Trailing Vortex.

The theoretical tangential velocity induced by a potential trailing vortex has a singularity at the center of the vortex, and there are several historical core models available to represent the viscous core of the vortex. The vortex core diameter for this analysis was varied from 1% to 3% of the DC-8 span.

Two possible models for the velocity profile through the vortex core are the Lamb-Oseen model and the Burnham-Hallock model,[4-6] and examples of the two velocity profiles are shown in Fig. 2 for a core radius equal to 1% of the DC-8

wing span. The Burnham-Hallock model with a core diameter of 1.5% of the DC-8 wing span was used for most of the results presented below.

The strength of the trailing vortex decays with distance aft of the generating aircraft. A three-phase model of vortex strength decay as a function of distance behind the DC-8 (weak decay in the near field, followed by rapid decay as the vortices roll up, followed by gradual decay in the mid and far field) was based on the results described in Refs. 4-6.

The DC-8 trailing vortex field for a nominal flight condition is shown in Fig. 3. Vectors represent velocity components in the Y-Z plane at the DC-8 tail location. Colors represent these vector component values relative to the free-stream velocity. This is the typical flow field through which the Falcon must fly during the flight tests.

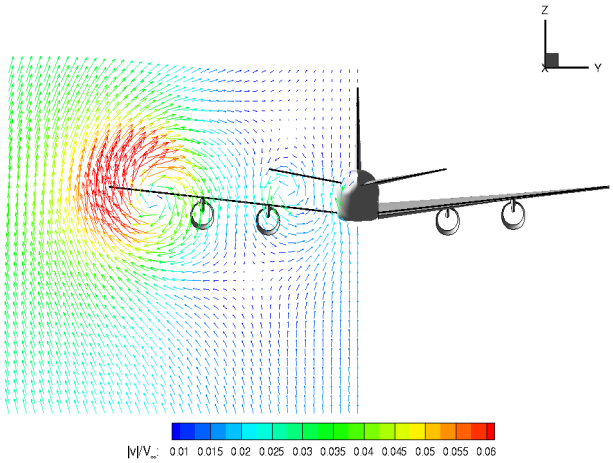

Figure 3. Velocity Flow Field Behind the Model DC-8.

2.3 Aerodynamic Prediction Methods

The predicted aerodynamic loads were obtained using the Nielsen Engineering and Research (NEAR) aerodynamic prediction codes: the STRLNCH store separation analysis tools[7-10] and the Missile Distributed Loads (MISDL) codes.[11-17] These codes have been validated with flight data for numerous applications, and they have the advantage of being fast running and suitable for the large number of simulations required.

The MISDL code was used to model both the DC-8 and Falcon aircraft. The DC-8 was modeled to determine its trailing vortex wake at trimmed flight conditions. The Falcon was modeled to predict the aerodynamic loads acting on it in the free stream and when immersed in the trailing wake of the DC-8 aircraft. MISDL is a singularity and panel-method-based aerodynamic prediction method, which includes high-angle-of-attack body and lifting surface vortex models, rotational rates, and nonuniform flow effects. MISDL uses classical singularity methods augmented with body and fin vortex modeling, and wing stall models based on empirical data.

2.4 Trajectory Simulation Method

The NEAR STRLNCH aircraft store separation simulation code[7-10] was used to model and predict 6-DOF uncontrolled (stick-fixed) trajectory characteristics of the Falcon aircraft starting at selected positions directly behind the DC-8. STRLNCH can model flow effects due to combined angle of pitch and sideslip, as well as rotational rates. The aerodynamic prediction methods described above were used to model Falcon aerodynamic forces and moments for the simulations. A breakdown of forces and moments on each aircraft component during the flight simulation is available to determine vortex-induced forces and moments. For each simulation, the Falcon is trimmed for the selected flight path at the starting point. It is released with no control inputs during the simulation, and each trajectory simulation is run for a fixed time or until the aircraft is out of the influence of the DC-8 trailing wake.

3.0 RESULTS

The objectives of this investigation were to identify the maximum static induced loads on the Falcon in close encounters with the DC-8 wake, determine an envelope of safe trail distances behind the DC-8, provide an indication of the flight dynamics of the Falcon in the DC-8 wake, and determine the history of

the Falcon component loads during the dynamic maneuver. A small sampling of the predicted results from this study is presented below.

3.1 Static Loads

The static loads on the Falcon were predicted at a matrix of locations aft of the DC-8 at a specified test flight condition. Overall vortex-induced aerodynamic loads on the aircraft and component loads and bending moments were obtained for many flight conditions and trail distances behind the DC-8. The Falcon, in a free-stream cruise trim attitude, was placed in the trailing vortex field, and the static aerodynamic characteristics in the nonuniform velocity field were calculated. Contour maps in a plane normal to the DC-8 longitudinal axis proved an expedient way to illustrate the locations of maximum induced loads.

Results in Figs. 4-8 are interpreted as follows: placing the Falcon nose, represented by the black dot on the outline of the aircraft, at a point on the y-z plane aft of the DC-8 shows the wake-induced aerodynamic coefficient on the Falcon. For example, in Fig. 4, if the nose of the Falcon is placed at the y-z location (-60,0), which is near the centroid of the DC-8 trailing vortex, the induced rolling moment coefficient on the Falcon is approximately 0.28, right wing down. This presentation of results permitted a rapid evaluation of the location of large wake-induced effects on the Falcon and the regions of large aerodynamic gradients.

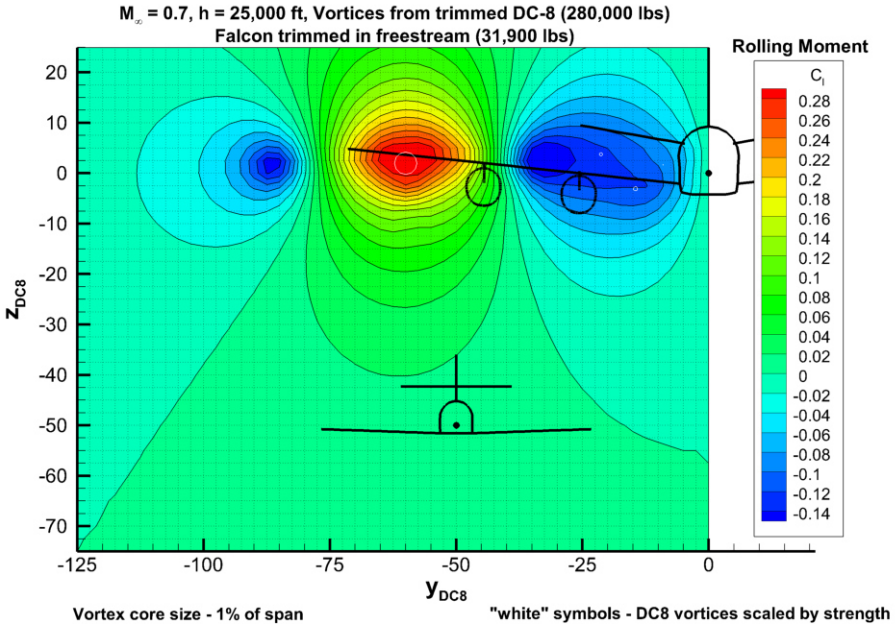

Figure 4. Induced Rolling-Moment Coefficient (C_l).

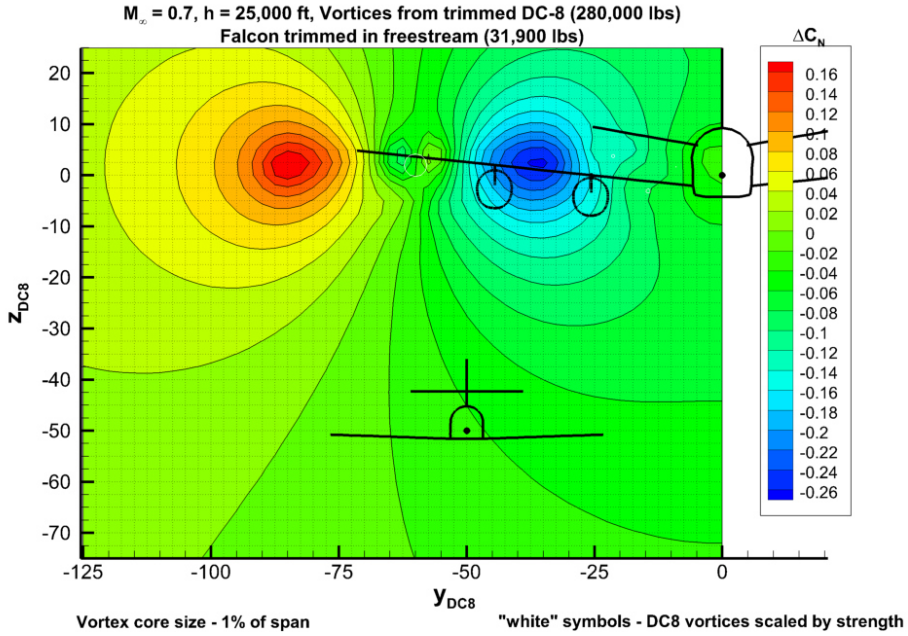

Figure 5. Induced Normal-Force Coefficient (ΔC_N).

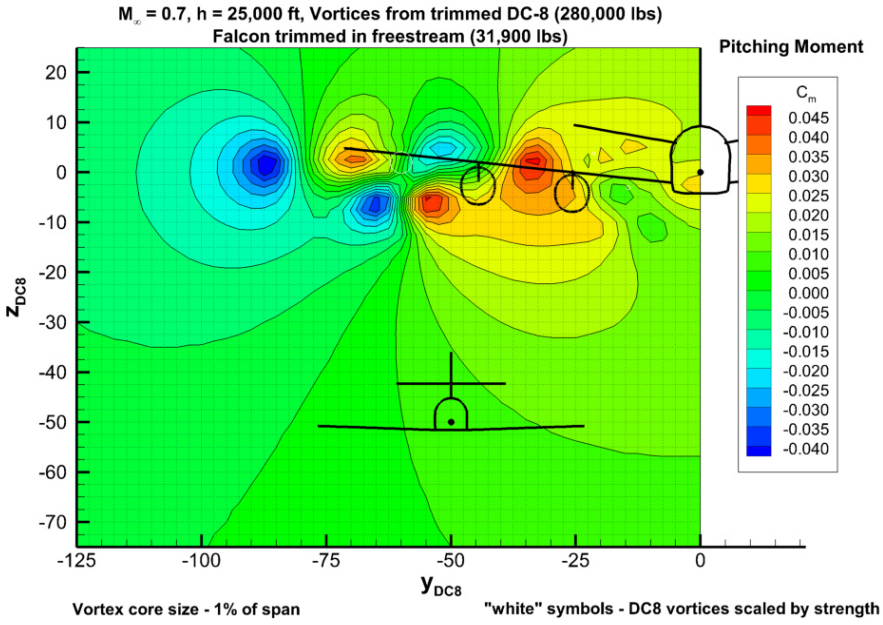

Figure 6. Induced Pitching-Moment Coefficient (C_m).

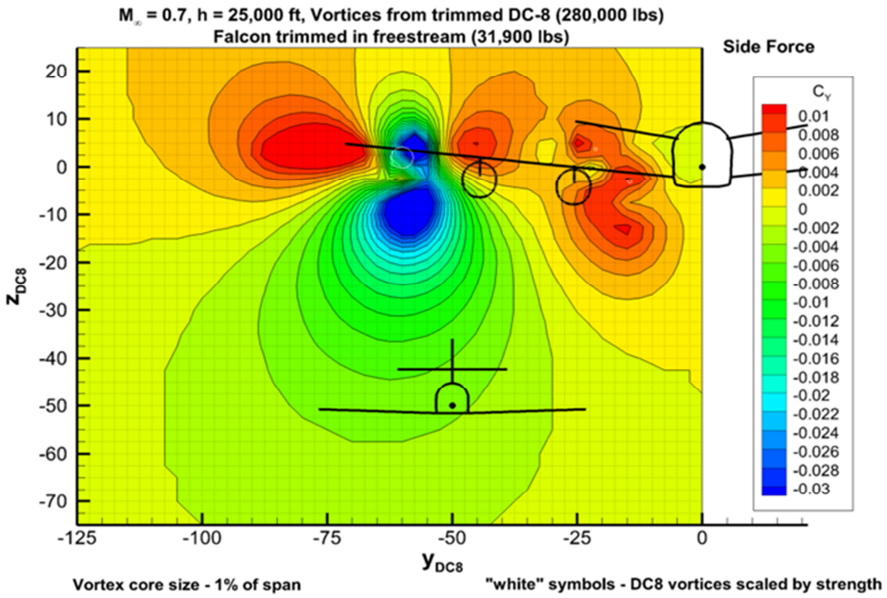

Figure 7. Induced Side-Force Coefficient (ΔC_Y).

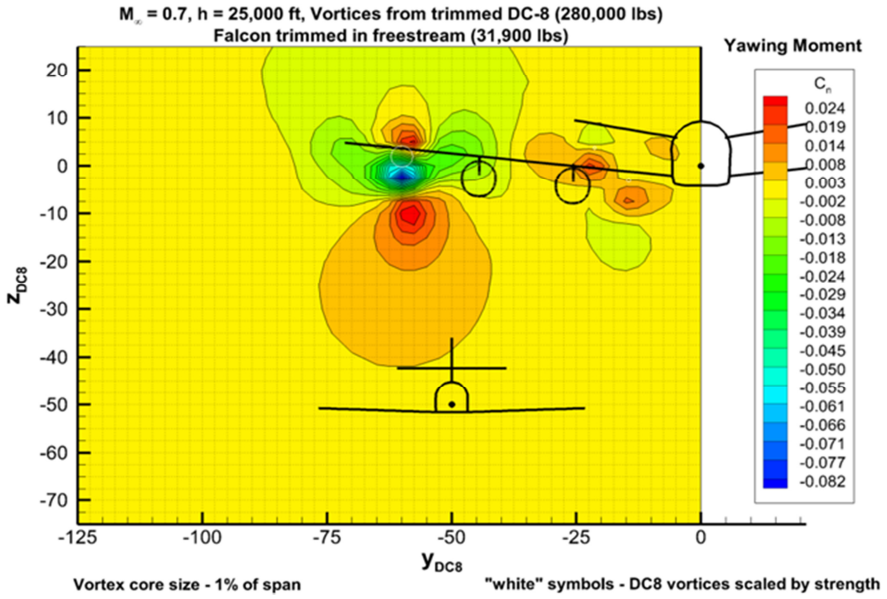

Figure 8. Induced Yawing-Moment Coefficient (ΔC_n).

Similar contour maps were generated for the induced normal forces and bending moments on the Falcon's aerodynamic surfaces for the airplane at a matrix of locations behind the DC-8. Figures 9-12 illustrate the induced normal-force and bending-moment coefficients on the Falcon's right and left horizontal tail surfaces at a nominal flight-test condition for the DC-8. This presentation of the Falcon component loads permitted rapid evaluation of the locations of high induced loads and bending moments.

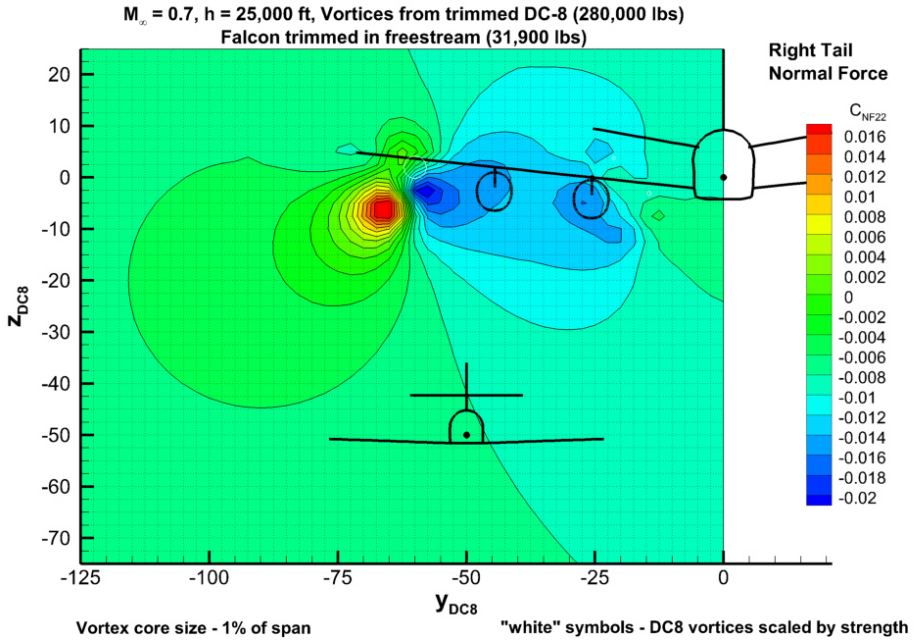

Figure 9. Near-Field Map of Falcon Right Horizontal Tail Normal-Force Coefficient (C_{NF22}).

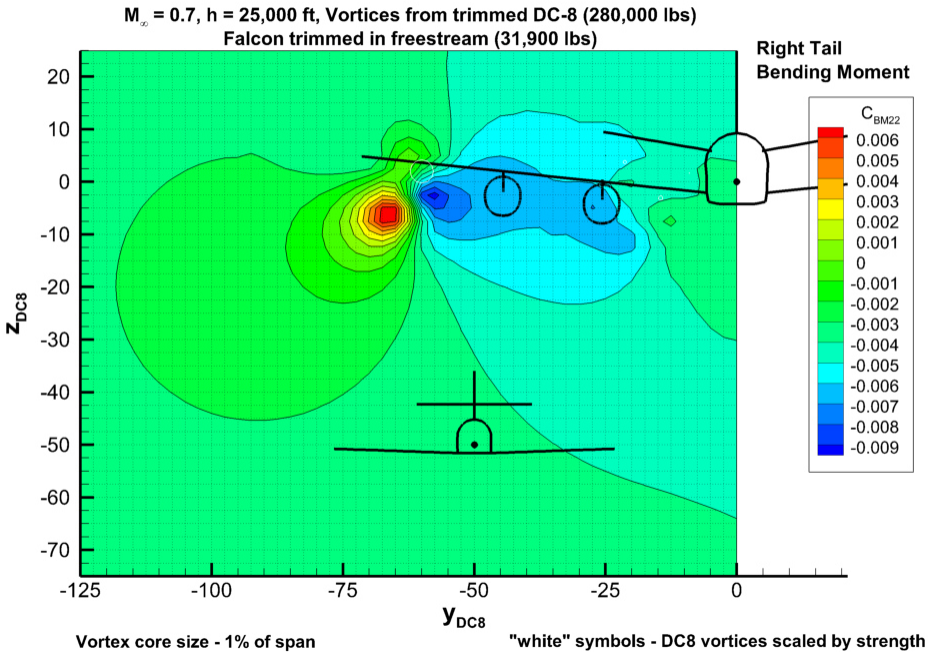

Figure 10. Near-Field Map of Falcon Right Horizontal Tail Bending-Moment Coefficient (C_{BM22}).

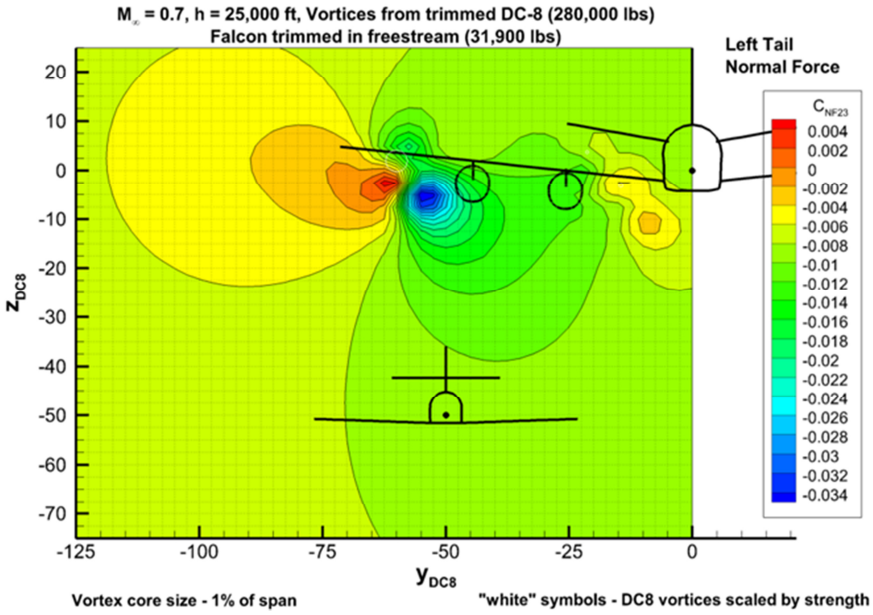

Figure 11. Near-Field Map of HU-25C Left Horizontal Tail Normal-Force Coefficient (C_{NF23}).

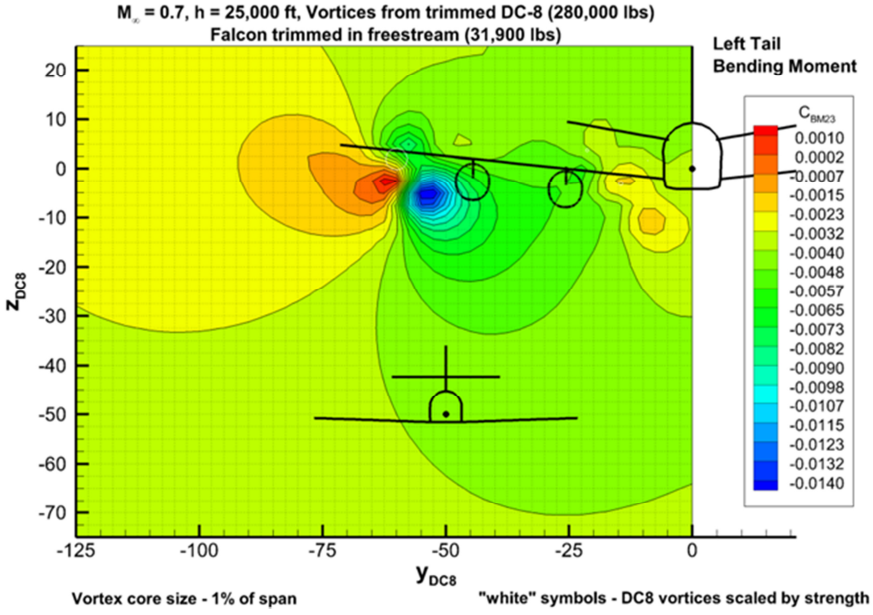

Figure 12. Near-Field Map of HU-25C Left Horizontal Tail Bending-Moment Coefficient (C_{BM23}).

3.2 Dynamic Simulations

Dynamic 6-DOF trajectory simulations of the Falcon traversing the DC-8 wake were made to study the differences between horizontal and vertical traverses. First, it was important to understand if there was a difference in component vortex-induced loadings for the horizontal and vertical traverses. Second, it was of interest to understand the reaction of the Falcon to a close encounter with a strong trailing vortex to forewarn the pilots of possible extreme flight conditions.

The original flight test plan called for a vertical traverse of the DC-8 trailing vortex with the Falcon descending through the vortex from above. The aircraft was trimmed at an initial position 100 ft. above

the trailing vortex such that it would descend at a 2-degree flight path angle upon release. It would descend, stick-fixed, into the vortex or wherever the induced flow field dictated it to go. The release point above the vortex was varied from directly above the DC-8 trailing vortex (y=-60 ft.) to approximately 35 ft. outboard of the vortex (y=-95 ft.). All trajectories were run for approximately seven seconds. The position of the Falcon is shown every 0.5 seconds to illustrate the trajectory in Figs. 13-15. Trail distance of 0 nm was used for these trajectory simulations because trajectories will be more benign at greater trail distances.

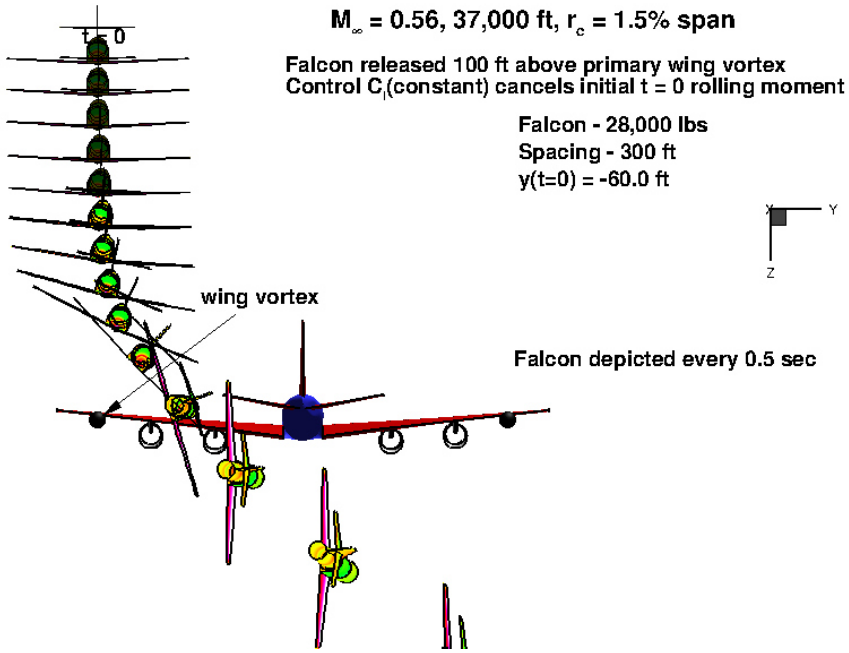

Figure 13. HU-25 Vertical Traverse, y = -60 ft.

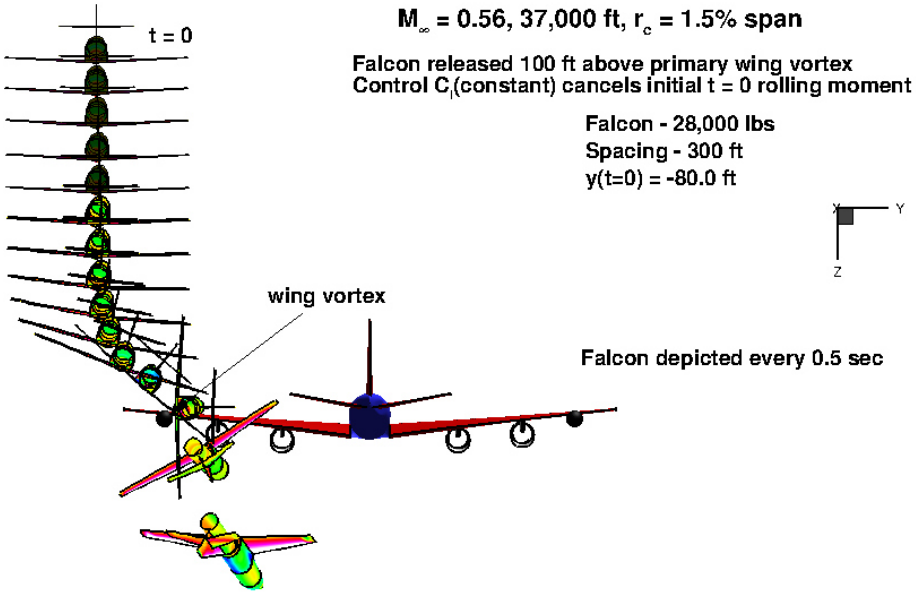

Figure 14. HU-25 Vertical Traverse, y = -80 ft.

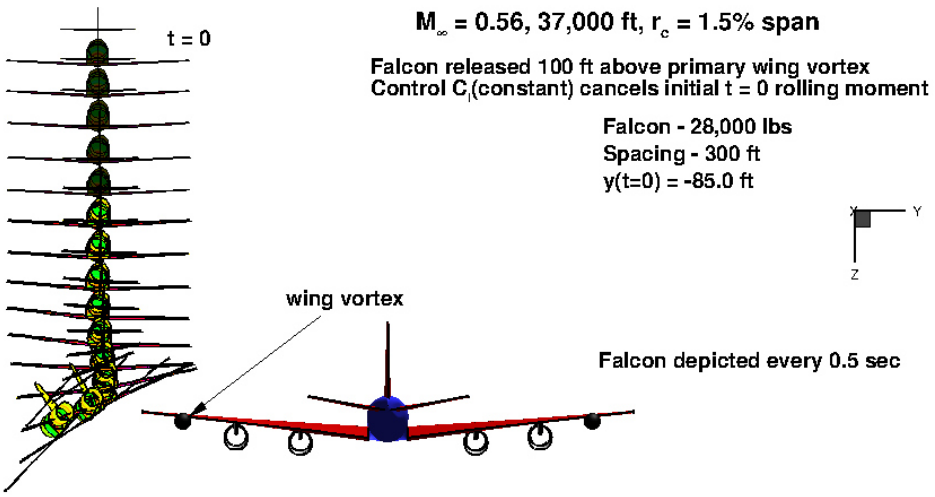

Figure 15. HU-25 Vertical Traverse, y = -85 ft.

A similar parametric study of lateral flight traverses through the trailing vortex was conducted. The Falcon was trimmed at the specified heading angle, six degrees toward inboard for the results shown below, at an initial location approximately 100 ft. outboard of the DC-8 trailing vortex (y = -160 ft.), and at vertical positions between 5-ft. above the vortex to 5-ft. below the vortex. The stick-fixed trajectory simulations were run as before, and the lateral trajectory simulations are shown in Figs. 16-18.

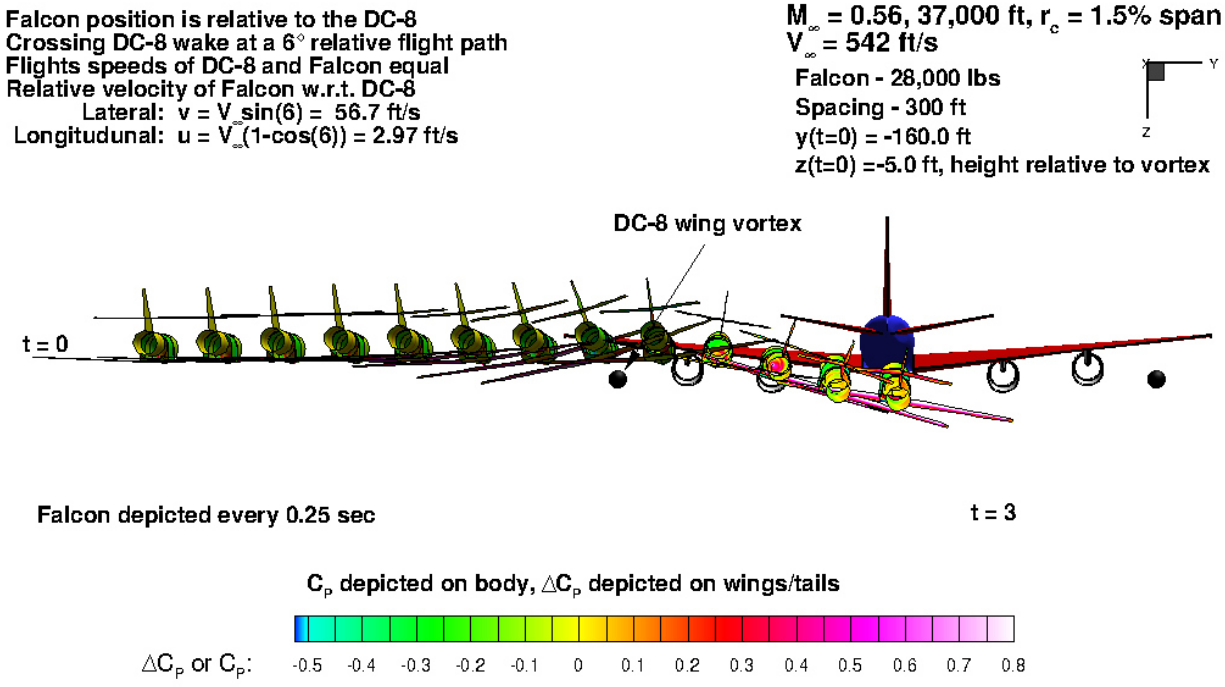

Figure 16. HU-25 Lateral Traverse, 6-Degree Heading, 5-ft. Above the Vortex

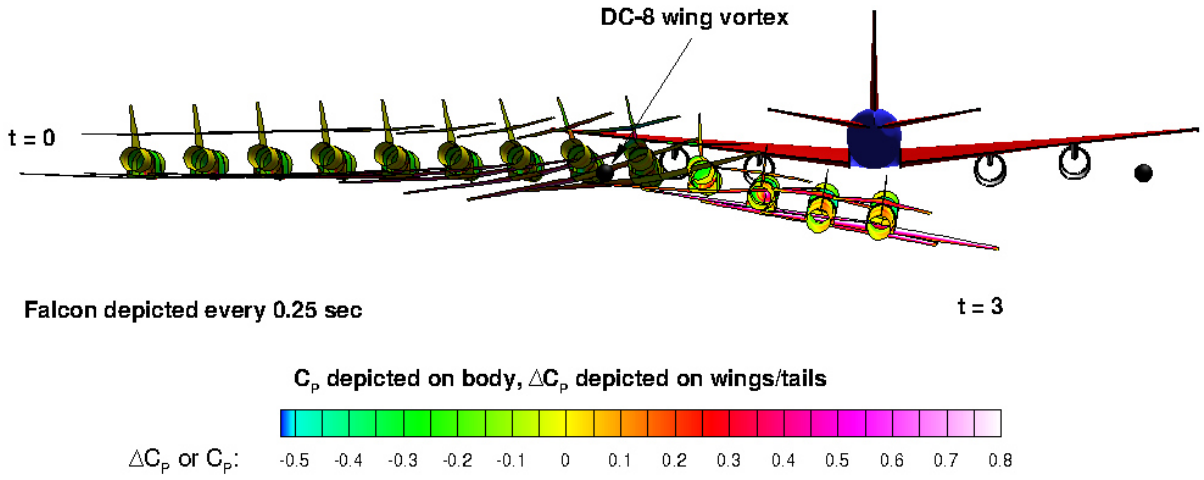

Figure 17. HU-25 Lateral Traverse, 6-Degree Heading, 0-ft. Above the Vortex.

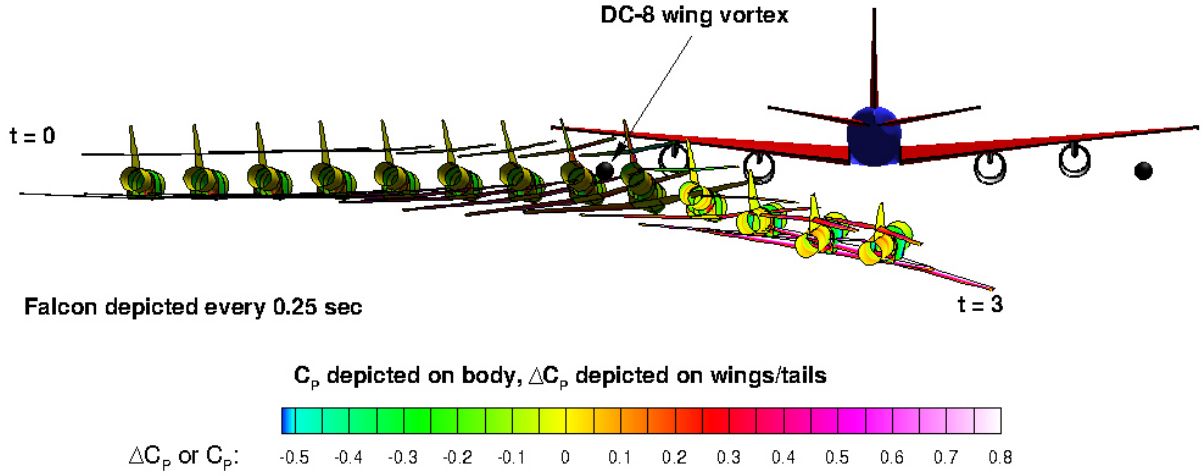

Figure 18. HU-25 Lateral Traverse, 6-Degree Heading, 5-ft. Below the Vortex.

For each of the trajectory simulations, the time history of the aircraft flight conditions and attitude, the overall aerodynamic forces and moments, and the aircraft component loads and bending moments are available. Examples for one vertical traverse and one lateral traverse are shown in Figs. 19 and 20, respectively.

The details of the Falcon motion and attitude during a vertical descent in Fig. 19 correspond to the trajectory shown in Fig. 13. The Falcon experiences large changes in yaw angle and in roll angle, but the angle of attack shows very little change. The maximum roll rate approaches 60 degrees/second. In Fig. 20 the Falcon motion during a much more benign lateral trajectory, shown in Fig. 17, is illustrated for comparison. The root bending moments on the vertical and horizontal tails and the tail junction are shown in this figure to illustrate the rapid changes that can be experienced during wake traverses.

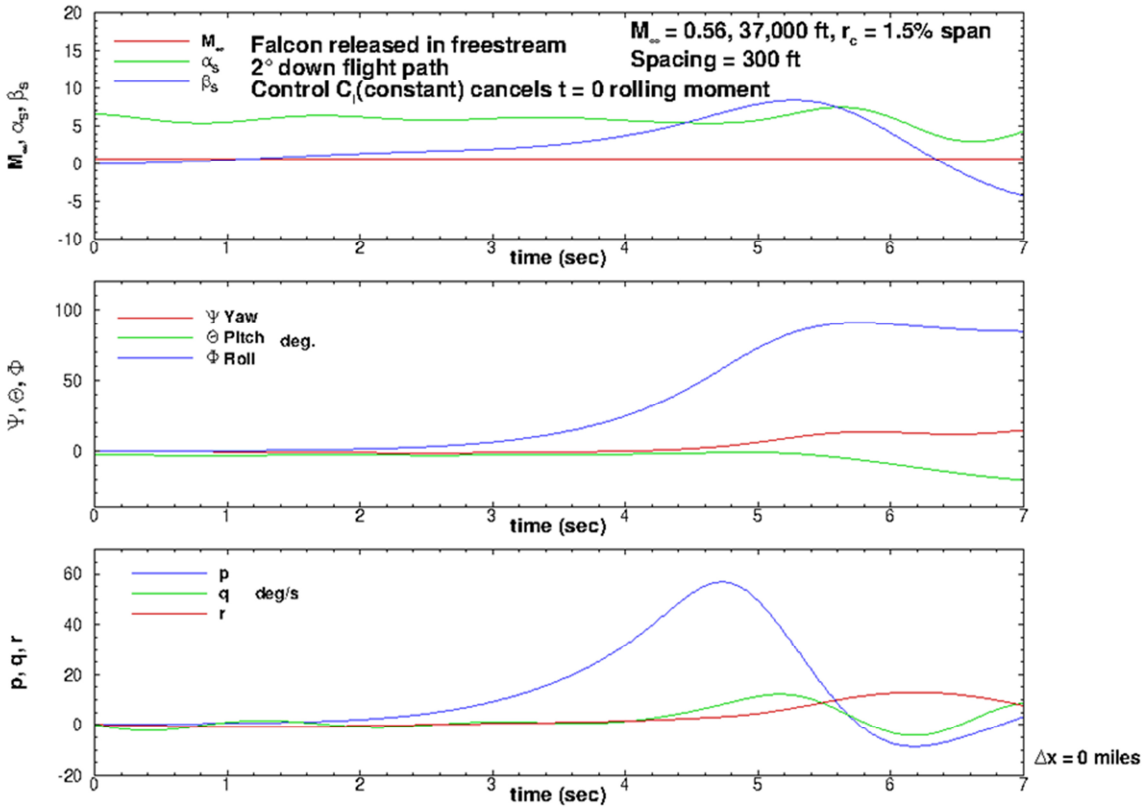

Figure 19. Falcon Vertical Traverse, 2-Degree Descent, Y(0)=-60 ft., Z(0)=100 ft.

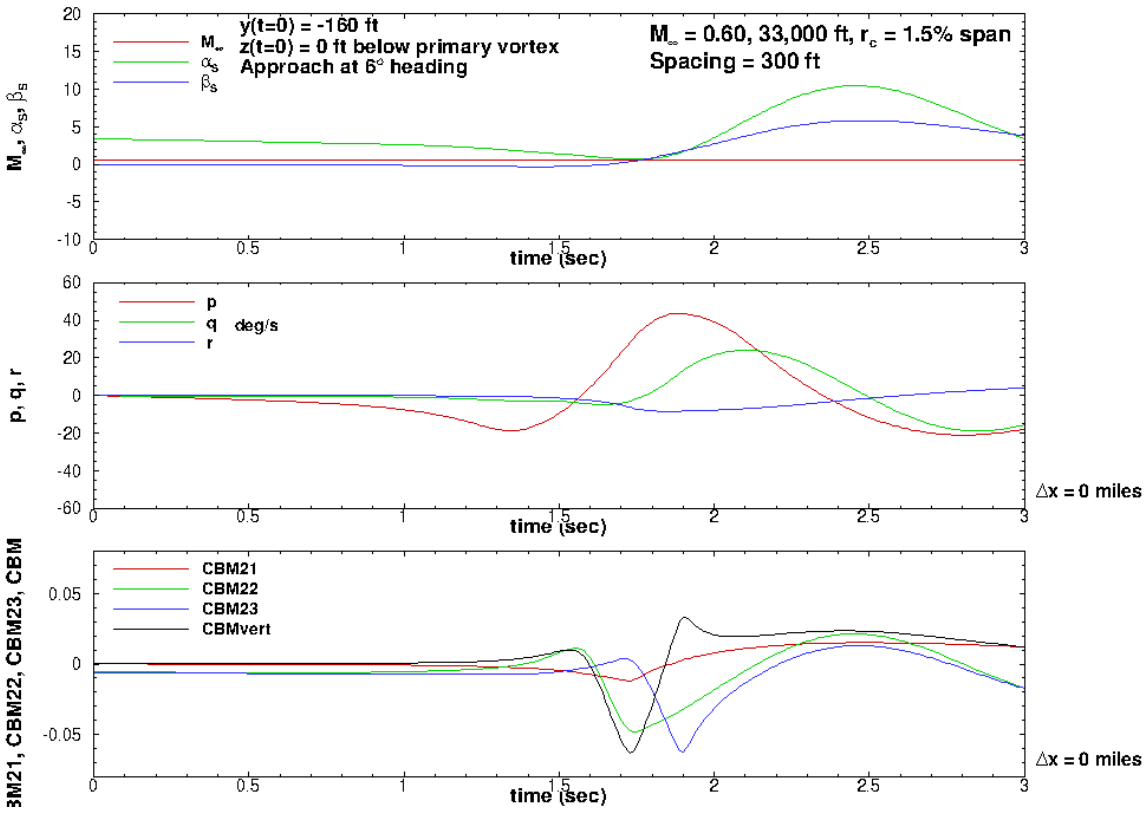

Figure 20. Falcon Lateral Traverse, 6-Degree Heading, Z(o)=0 ft.

3.3 Safe Trail Distance

The safe trail distance aft of the DC-8 was defined as that distance for which the maximum bending moment on the Falcon tail does not exceed 70% of the design limit load. Based on the static loading analyses, the maximum tail bending moments occurred when the primary DC-8 vortex was near the four nominal positions shown in Fig. 21. The maximum bending moments used to determine a safe trail distance were taken from the static loads predictions on the Falcon tail aft of a heavy and a light DC-8.

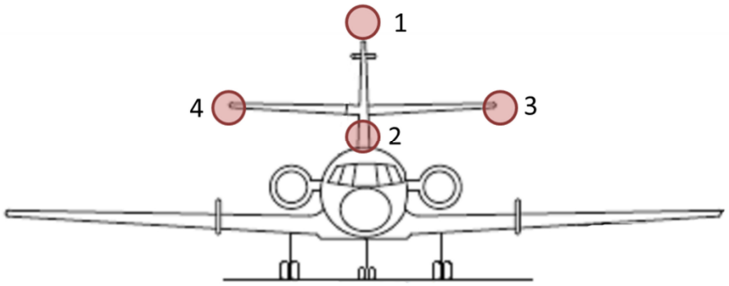

Figure 21. Trailing Vortex Positions for Trail Distance Validation.

For the results to follow, the DC-8 weights are 170,000 and 230,000 lbs, and the flight conditions are Mach 0.6 at 33,000 ft. The maximum Falcon empennage root bending moments for the primary DC-8 vortex in positions 1 through 3 are shown in Figs. 22-24, respectively. Note that 70% DLL is shown as the green dashed line. The maximum horizontal tail junction bending moments for the three vortex locations are shown in Figs. 25-27.

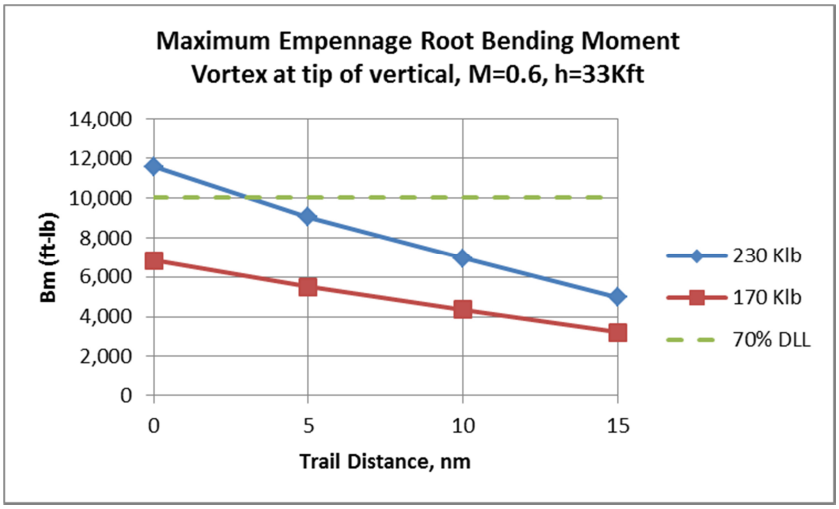

Figure 22. Maximum HU-25C Empennage Root Bending Moment, Vortex Position 1.

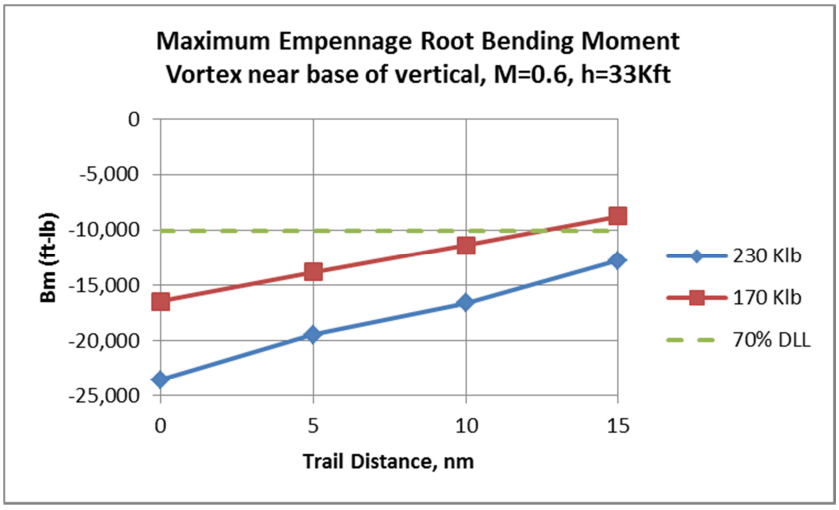

Figure 23. Maximum HU-25C Empennage Root Bending Moment, Vortex Position 2.

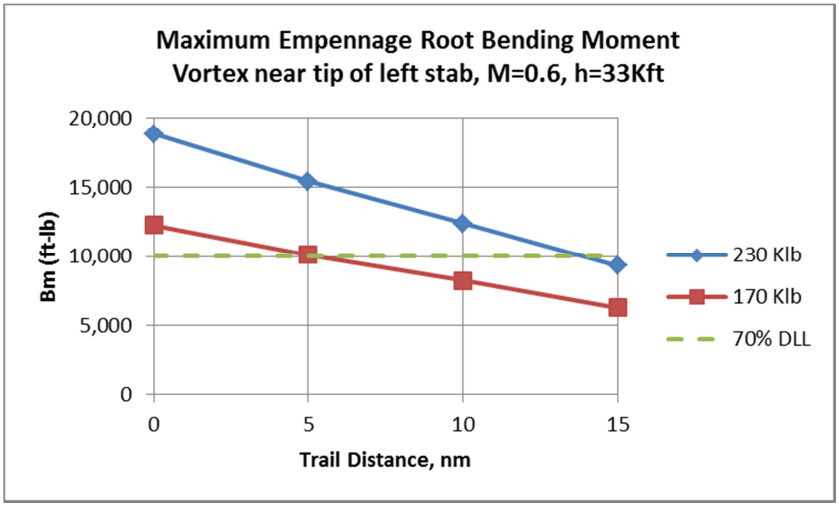

Figure 24. Maximum HU-25C Empennage Root Bending Moment, Vortex Position 3.

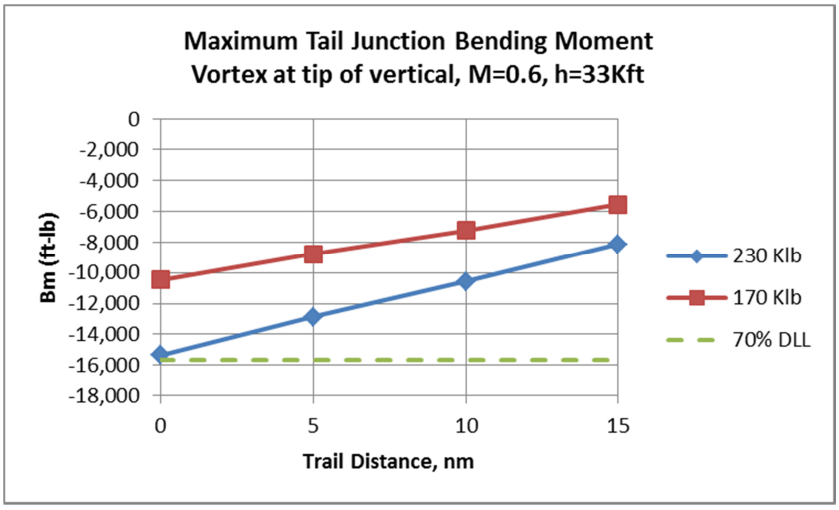

Figure 25. Maximum HU-25C Tail Junction Bending Moment, Vortex Position 1.

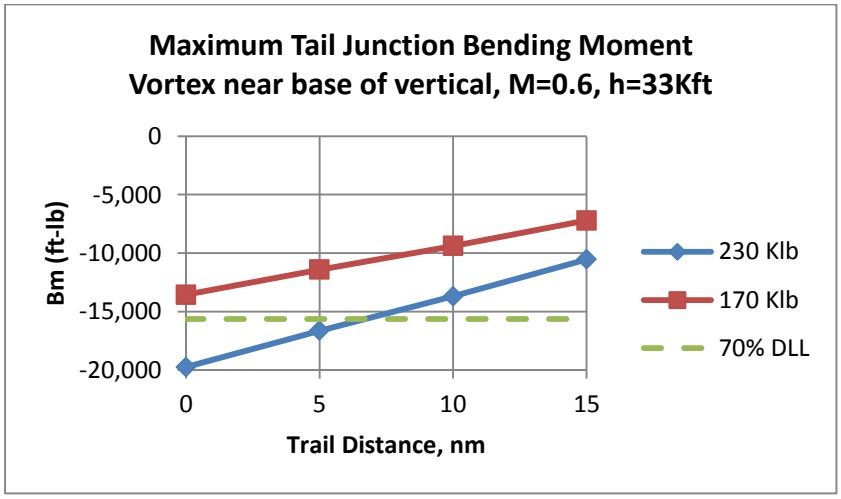

Figure 26. Maximum HU-25C Tail Junction Bending Moment, Vortex Position 2.

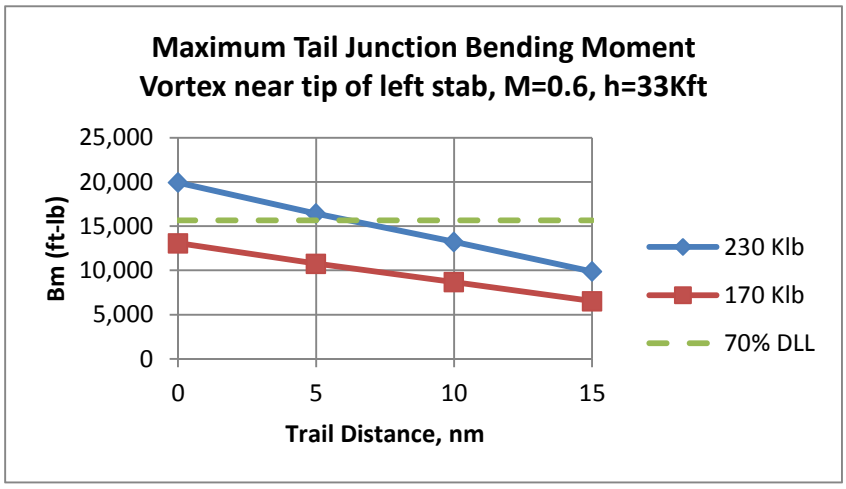

Figure 27. Maximum HU-25C Tail Junction Bending Moment, Vortex Position 3.

These results verified the ACCESS project team estimate of 15 nm as a safe trail distance; however, they were also less conservative than the project estimates and showed much closer safe trail distances for certain trailing vortex positions with respect to the Falcon tail.

3.4 Flight Data Comparisons

Falcon attitude data were measured on some flights during the wake traverses, and all traverses were made laterally through the vortex. Unfortunately, the precise location of the Falcon with respect to the primary DC-8 vortex is not known, so the comparison of predicted aircraft characteristics during the close interaction with the vortex can only be qualitative in nature. The roll angle results are shown in Fig. 28 below.

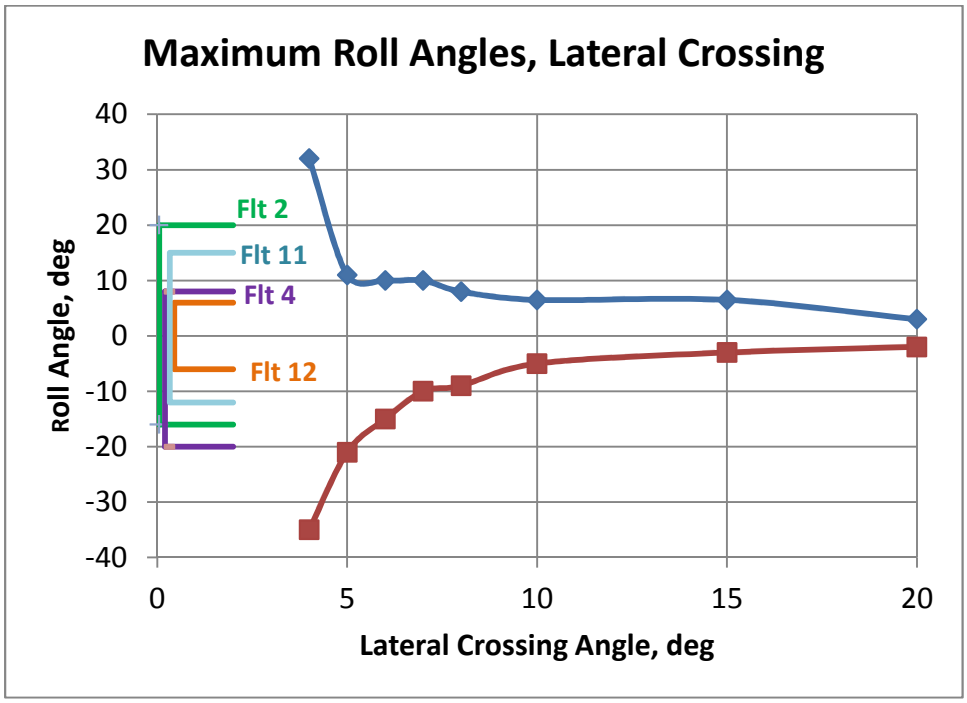

Figure 28. Maximum HU-25C Vortex-Induced Roll Angles, Predictions vs Flight.

In Fig. 28, the predicted maximum vortex-induced positive and negative roll angles for the Falcon at the same vertical level as the primary vortex are shown for varying lateral crossing angles. (see Fig 17) For each of the four flight tests examined, in which 15-25 individual crossings were made, the range of roll angles measured is illustrated by the brackets. Notice that the maximum roll angles experienced during the traverses are always in the range predicted a priori. There are not sufficient data available to get an exact comparison for each individual traverse.

4.0 CONCLUSIONS AND DISCUSSION

The static loads analyses described in this paper corroborated previously-determined safe test flight trail distances, and the test flights were conducted safely. The flight characteristics experienced by the Falcon trailing aircraft during DC-8 vortex traverses were consistent with the dynamic simulation predictions according to pilot comments. The simulation results shown above, that a lateral traverse through the DC-8 vortex is more benign in pitch, roll, yaw, than a vertical traverse, dictated a change in the test flight procedures.

The results of this analysis demonstrate that reduced-order prediction methods are extremely useful for complex aerodynamic problems, particularly when it is necessary to analyze tens of thousands of discrete points defined by the flow conditions and the matrix of relative positions of the two aircraft and including dynamic 6-DOF simulations. The prediction method produced maximum vortex-induced roll angles that were within the range experienced in flight.

REFERENCES

1. ACCESS Web Site: http://www.nasa.gov/aero/access-II.html#.VPCdfOGsnVo
2. Mendenhall, M. R., Lesieutre, D. J., and Kelly, M. J.: "Trailing Vortex-Induced Loads During Close Encounters in Cruise," AIAA 2015-3300, June 2015.
3. Kelly, M. J., et al, "Probing Aircraft Flight Test Hazard Mitigation for the Alternative Fuel Effects on Contrails & Cruise Emissions (ACCESS) Research Team," NESC-RP-12-00822 Vol. 1 and 2, April 18, 2013.
4. Proctor, F. H., Ahmad, N. N., Switzer, G. S., Limon Duparcmeur, F. M.: "Three-Phased Wake Vortex Decay," AIAA 2010-7991, August 2010.
5. Ahmad, N. N., Proctor, F. H., Duparcmeur, F. M. L., and Jacob, D.: "Review of Idealized Aircraft Wake Vortex Models". AIAA 2014-0927, January 2014.
6. [3]Gerz, T., Holzapfel, F. and Darracq, D., "Commercial Aircraft Wake Vortices," *Progress in Aerospace Sciences*, Vol. 38, p.181-208, 2002.
7. Lesieutre, D. J. and Perkins, S. C., Jr., "Store Separation Prediction Program *STRLNCH*, Version March 2013", NEAR TR 655, March 2013.
8. Dillenius, M. F. E., Love, J. F., Hegedus, M. C., and Lesieutre, D. J., "Program *STRLNCH* for Simulating Missile Launch from a Maneuvering Parent Aircraft at Subsonic Speed," NEAR TR 509, 1996.
9. Dillenius, M. F. E., Goodwin, F. K., and Nielsen, J. N., "Analytical Prediction of Store Separation Characteristics from Subsonic Aircraft," *Journal of Aircraft*, Vol. 12, No. 10, October 1975, pp. 812-818.
10. Dillenius, M. F. E., Goodwin, F. K., and Nielsen, J. N., "Extension of the Method for Predicting Six-Degree-of-Freedom Store Separation Trajectories at Speeds up to the Critical Speed to Include a Fuselage with Noncircular Cross Section, Volume I - Theoretical Methods and Comparisons with Experiment," AFFDL-TR-74-130, March 1974.
11. Lesieutre, D. J., "Detailed Aerodynamic Prediction Program MISDL, Code User's Manual, Version October 2013," NEAR TR 651, October 2013.
12. Lesieutre, D. J. and Quijano, O. E., "Studies of Vortex Interference Associated with Missile Configurations," AIAA-2014-0213, January 2014.
13. McDaniel, M. A., Evans, C. and Lesieutre, D. J., "The Effect of Tail Fin Parameters on the Induced Roll of a Canard-Controlled Missile," AIAA 2010-4226, June 2010.
14. Lesieutre, D. J., Dillenius, M. F. E., and Lesieutre, T. O., "Multidisciplinary Design Optimization of Missile Configurations and Fin Planforms for Improved Performance," AIAA-1998-4890, September 1998.
15. Lesieutre, D. J., Dillenius, M. F. E., Love, J. F., and Perkins, S. C., Jr., "Nonlinear Engineering-Level Missile Aerodynamics Prediction Methods *MISL3*, *MISDL*, and *NEARZEUSIN/ZEUSBL*," CEAS Aerospace Aerodynamics Research Conference, London, UK, June 10–12, 2003.
16. Lesieutre, D. J., Love, J. F., and Dillenius, M. F. E., "Prediction of the Nonlinear Aerodynamic Characteristics of Tandem-Control and Rolling-Tail Missiles," AIAA 2002-4511, August 2002.
17. Dillenius, M. F. E., Lesieutre, D. J., Hegedus, M. C., Perkins, S. C., Jr., Love, J. F., and Lesieutre, T. O., "Engineering-Intermediate-, and High-Level Aerodynamic Prediction Methods and Applications," *Journal of Spacecraft and Rockets*, Vol. 36, No. 5, Sep.-Oct. 1999, pp. 609-620.